Korean J. Chem. Eng., 35(8), 1735-1740 (2018)
DOI: 10.1007/s11814-018-0083-z

pISSN: 0256-1115
eISSN: 1975-7220

A visible-light-active $BiFeO_3$/ZnS nanocomposite for photocatalytic conversion of greenhouse gases

Nasim Bagvand, Shahram Sharifnia†, and Elham Karamian

Catal. Res. Cen., Chem. Eng. Department, Razi University, Kermanshah 67149-67246, Iran
(*Received 6 February 2018 • accepted 11 May 2018*)

Abstract−Given the changes in environmental conditions in the world, photocatalytic conversion of greenhouse gases is of great interest today. Our aim was to increase the photocatalytic efficiency of $BiFeO_3$/ZnS (p-n heterojunction photocatalyst) by varying the molar ratio of ZnS to perovskite structure of $BiFeO_3$ using hydrothermal synthesis. The results of X-ray diffraction (XRD), scanning electron microscopy (SEM), energy dispersive spectroscopy (EDS), FT-IR spectroscopy showed the small crystal size and suitable distribution of ZnS particles on the $BiFeO_3$ structure. The results of UV-visible, and photoluminescence (PL) spectroscopy analyses showed the good behavior of p-n heterostructure in absorption of visible light and lowering electron-hole recombination. The best visible light photocatalytic efficiency of CO_2 reduction, 24.8%, was obtained by an equimolar ratio of $BiFeO_3$/ZnS.

Keywords: Photocatalytic Conversion, Greenhouse Gases, p-n Heterojunction, $BiFeO_3$ Perovskite, ZnS

INTRODUCTION

In recent years, the greenhouse effect has caused many difficult environmental problems [1]. The greenhouse effect is caused by increased emanation of greenhouse gases, such as carbon dioxide, and methane. Evidently, the increase in greenhouse gasses will change environmental patterns and contribute to the rise of global warming. Photocatalytic reduction of CO_2 using solar radiation to other useful carbon-based compounds is a promising route for recycling carbon materials [2,3].

Photocatalysts are frequently used for degrading pollutants either in the visible or ultraviolet light range. Perovskite-based photocatalysts are an important category of semiconductors activating in both visible and UV light irradiation [4-6]. Coupling the photocatalysts is one of the strategies for upgrading the photo-activity of them, as the pure photocatalysts often show a limited efficiency.

Perovskite structure of $BiFeO_3$ is a photocatalyst with a narrow band gap of about 2.5 eV and shows multiferroic behavior [7,8], which can be well activated by receiving visible photons [9]. The holes generated in this photocatalyst are often suitable for oxidation of various organic pollutants. However, electrons do not have the potential for injection to CO_2 or reduction of silver cations.

ZnS is a photocatalyst with a wide band gap (3.4 eV) which is well activated by UV photons. The excited electrons of conduction band of ZnS are energetic enough to reduce the stable molecules of CO_2 [10]. Moreover, the life time of generated charge carriers in ZnS is more than that of $BiFeO_3$ because the higher band gap of ZnS reduces the effect of inner electric field for attraction and recombination of opposite charges.

So far, some studies have been conducted on the effect of $BiFeO_3$ as a p-type photocatalyst coupled with an n-type one for degradation of various organic pollutants. Zhang et al. [11] reported on the photocatalytic activity of TiO_2/$BiFeO_3$ under visible light to reduce silver cations in an aqueous environment. They attributed the appropriate photocatalytic activity TiO_2/$BiFeO_3$ to multi-fractional properties of $BiFeO_3$ as well as the effect of p-n binding between them. Ramadan et al. [12] conducted a study to investigate the positive effects of p-n photocatalytic compound, $BiFeO_3$/Fe_2O_3, on methylene blue degradation. The results showed an increase in the efficiency of charge separation, and they concluded that the construction of p-n structure causes an internal electric field leading to the transfer of charge carriers on opposite direction.

The main aim of this study was to construct a visible-light-active coupling photocatalyst for which its photocatalytic activity is higher than that of each pure one. For the first time, we used $BiFeO_3$/ZnS for the study of direct photocatalytic reduction of CO_2 under visible light. ZnS and $BiFeO_3$ nanoparticles were synthesized through precipitation and hydrothermal methods, respectively. Next, the various molar ratios of these photocatalysts were synthesized to assess the photocatalytic reduction of gaseous CO_2 in the presence of CH_4 as a reducing agent under visible light.

EXPERIMENTAL

1. Synthesis of $BiFeO_3$

Equimolar ratios of bismuth nitrate and iron nitrate 1.01 g (1.2 g $Fe(NO_3)\cdot 9H_2O$ and 1.2 g $Bi(NO_3)\cdot 5H_2O$) were simultaneously dissolved in 20 mL of diluted nitric acid (HNO_3, 30%). Then, 200 mL of KOH (8.0 M) solution with a concentration of 8 mL was gradually added to the solution within a large magnetic stirrer (1,000 rpm) until reaching a homogeneous and uniform brown suspension. The obtained suspension was transferred into a stainless steel autoclave and incubated at 200 °C for 6 h and then cooled at ambient temperature. Using distilled water and ethanol, the obtained powder

†To whom correspondence should be addressed.
E-mail: sharif@razi.ac.ir

was washed several times and finally dried at 80 °C for 6 h.

2. Synthesis of ZnS

The co-precipitation method was used to prepare ZnS. Based on this method, first, 10 mL of 0.5 M zinc acetate dehydrate solution ($Zn(OAC)_2 \cdot 2H_2O$) along with 10 mL of 0.5 M sodium sulfide solution ($Na_2S \cdot 9H_2O$) were stirred on a stirrer. Then these two, in drops, were added into 10 mL of 0.5 M sodium dodecyl sulfate (SDS) and the solution was placed on a stirrer for 30 min to obtain a homogeneous solution. The obtained solution was then passed through a filter paper and washed with distilled water and ethanol; finally, the obtained precipitates were placed in the oven at 60 °C for 24 h [13].

3. Synthesis of $BiFeO_3$/ZnS

To prepare the couple of $BiFeO_3$/ZnS with different ratios, at the end of ZnS synthesis, the completely homogeneous $BiFeO_3$ powder was added to the solution and placed under ultrasonic (frequency 20 kHz, amplitude 3 mm) for 30 min. Then, it was filtered and washed with ethanol and distilled water. The obtained precipitates were dried at 80 °C for 24 h. In this study we synthesized and analyzed different molar ratios of $BiFeO_3$/ZnS including 1 : 1, 1 : 2, and 2 : 1, and denoted as BZ11, BZ12, and BZ21, respectively.

4. Photocatalytic Reduction of CO_2

Previous studies have widely investigated the effect of photocatalytic reduction of CO_2 in aqueous solutions under UV-Vis radiation. We used a laboratory system to investigate the performance of $BiFeO_3$ and ZnS photocatalytic compounds at various molar ratios on the conversion of greenhouse gases, including carbon dioxide and methane. The experiments were carried out in a steel reactor with an internal volume of one liter under visible light radiation. In each experiment, first webnets with a mesh size of 120 were coated with photocatalytic material and calcined at 350 °C for 2 h and then placed inside the reactor. In the next step, the reactor was vacuumed using a vacuum pump and then filled with a gas feed, which was a mixture of carbon dioxide, methane, and helium with a ratio of CO_2 (45%), CH_4 (45%), and He (10%). Before starting the reaction and turning on the light within the reactor, we analyzed the initial feed composition by gas chromatograph GC-CGCA-1 apparatus equipped with a thermal conductivity detector (TCD). These analyses were done isothermally at 50 °C using a parallel setup of two packed columns (Molecular sieve and Porapak Q). The source of the visible light radiation was a 125 W UV lamp with a high pressure mercury vapor (Osrum, Germany). A glass cover was placed around the lamp to filter and remove UV radiation. After analysis of the feed, the lamp was switched on and the catalyst surface was continuously exposed to the light for 5 h. During this time, the combinations of gases in the reactor were analyzed by the GC every one hour. For each test, first a control test was performed to determine the potential absorbance of CO_2 molecules on the photocatalyst. A sample of gas mixture for the GC was taken after 4 h in the reactor when the light was switched off; the results obtained in this stage were compared with the results obtained from the feed, and the absorption rate was calculated. The results showed that the amount of absorption was negligible. The amount of CO_2 conversion at any time was calculated using Eq. (1), where $\mathbf{CO_2^i}$ and $\mathbf{CO_2^t}$, respectively, are the amount of CO_2 at zero and **t** times:

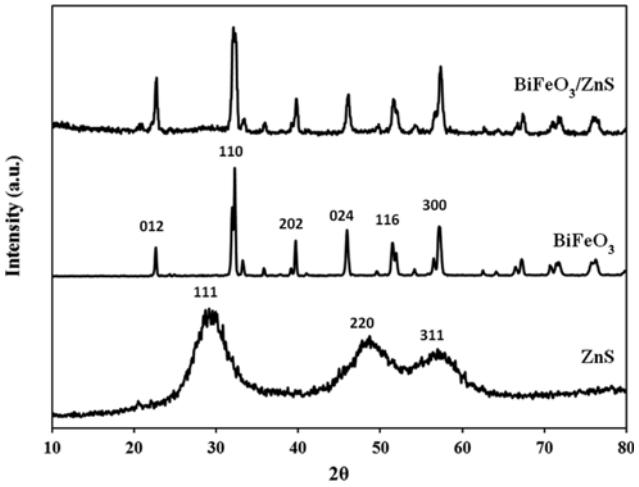

Fig. 1. The XRD patterns of ZnS, $BiFeO_3$, and BZ11 samples.

$$\mathbf{CO_2\ conversion\ percentage} = 100 \times \frac{\mathbf{CO_2^i - CO_2^t}}{\mathbf{CO_2^i}} \quad (1)$$

RESULTS AND DISCUSSION

1. Material Characterization

Fig. 1 presents the XRD patterns of $BiFeO_3$, ZnS, and BZ11 samples. As shown, the hydrothermal and precipitation methods are suitable for synthesis $BiFeO_3$, Zns and their coupling. The XRD pattern of ZnS has a number of diffraction peaks in 2θ=57.52, 48.94, and 30.16° which were, respectively, related to (311), (220), and (111) faces of the hexagonal crystalline structure of ZnS Wurtzite [14]. Similarly, the $BiFeO_3$ pattern has a number of diffraction peaks in 2θ equal to 57.4, 51.58, 45.88, 39.7, 32.26, and 22.72° which were, respectively, related to (300), (116), (024), (202), (110), and (012) faces in the structure of $BiFeO_3$ [11]. It is believed that when the crystalline semiconductor network is more complete and has fewer structural defects or impurities, the mobility and length of penetration of charge carriers will be increased because the defects or impurities may act as trapping sites for electron-holes. Thus, the efficiency of photocatalytic activity may be improved by improving the charge carrier transfer process [15]. In the spectrum related to the equimolar ratio of $BiFeO_3$ and ZnS, the peaks associated with both photocatalysts appearing at three points, 2θ equal to 57.4, 50.14, and 32.1° corresponding to (311), (220), and (111) faces in ZnS and $BiFeO_3$, respectively. It indicates the concurrent presence of both photocatalysts of $BiFeO_3$ and ZnS in the BZ11 sample.

Fig. 2 shows the EDX and SEM images of $BiFeO_3$, ZnS, and BZ11 samples. As shown in Fig. 2(a), we observed the semi-spherical particles of the $BiFeO_3$ photocatalyst. The particle size distribution in this photocatalyst seems to be in the range of 200 nm to micron, which is clearly larger than ZnS particles (Fig. 2(b)). The SEM image of ZnS in Fig. 2(b) shows the nano-sheet morphology of ZnS synthesized by precipitation method. Fig. 2(c) presents the ZnS and $BiFeO_3$ photocatalyst in BZ11 composite. As shown, the ZnS particles are well distributed on the $BiFeO_3$ surface. More-

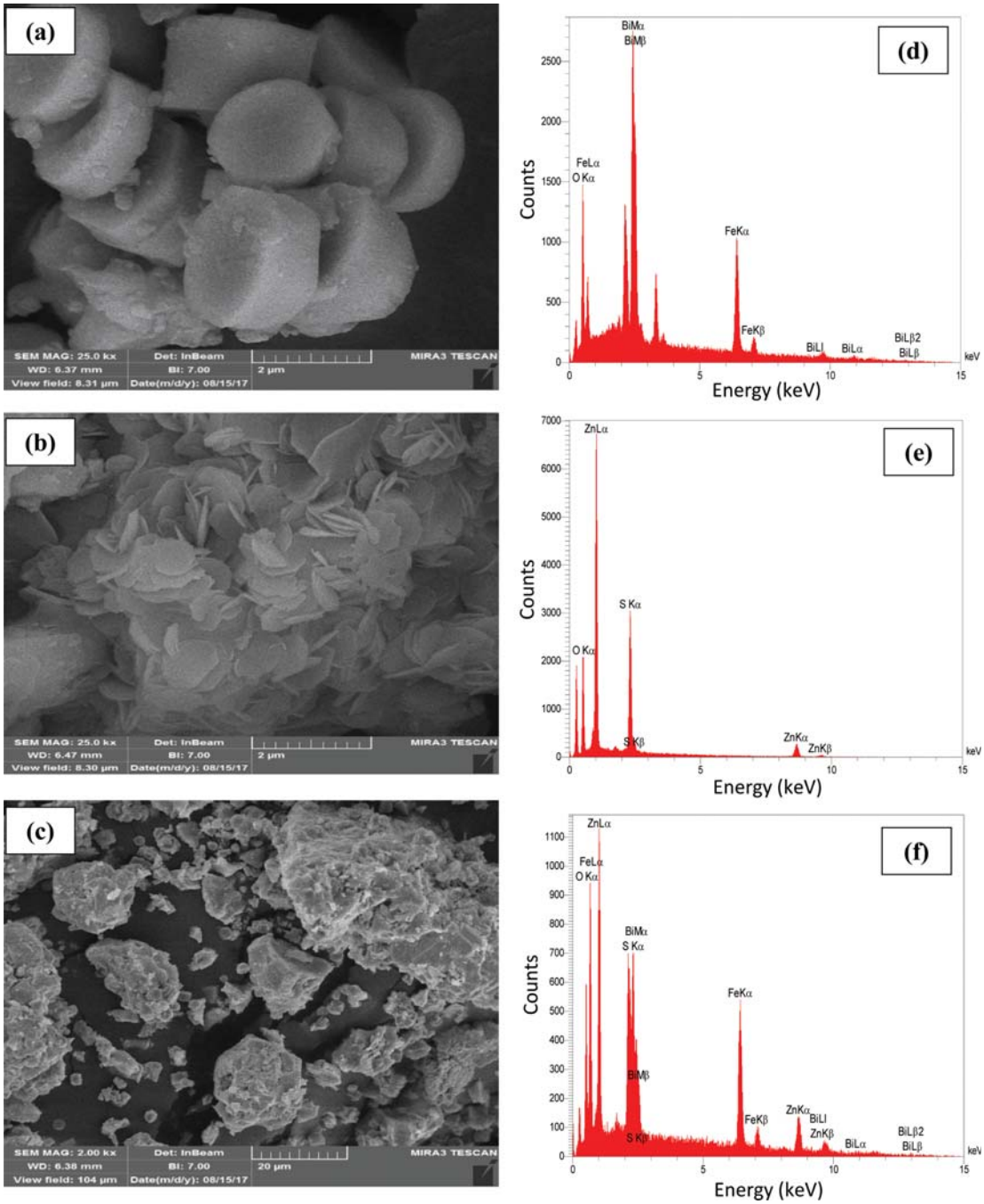

Fig. 2. The FESEM images and the EDX of (a), (d) $BiFeO_3$, (b), (e) ZnS, and (c), (f) BZ11.

Table 1. The EDX data for elemental composition of ZnS, $BiFeO_3$, and BZ11

Element	wt%		
	ZnS	$BiFeO_3$	BZ11
O	49.11	42.85	24.84
S	41.46	0	24.44
Fe	0	45.02	28.25
Zn	9.22	0	9.09
Bi	0	12.13	13.38

over, unique peaks appeared in the EDX spectrum of each of the photocatalysts, indicating the presence of Bi, Fe, Zn, S, O elements (Fig. 2(d)-(f)). The information of weight percent of each elements is presented in Table 1.

Fig. 3 presents the FTIR spectrum of $BiFeO_3$, ZnS, and their nanocomposites at room temperature. The ZnS characterization peaks of 1,221, 991 and 677 cm^{-1} are properly in line with the reported results of previous work [16,17]. As observed in $BiFeO_3$ perovskite peaks, there is a bending vibration of Fe-O-Fe at the range of 400-440 cm^{-1}. In addition, Bi-O bonds in the BiO_6 octahedral structure are observed at a range of 473-548 cm^{-1}, which is in line with the

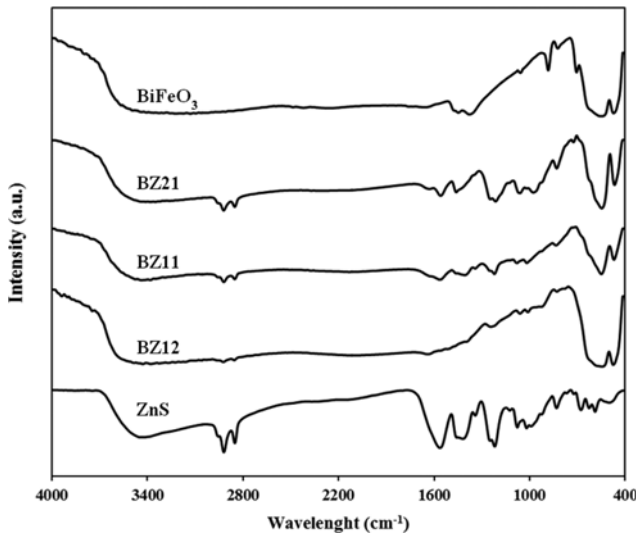

Fig. 3. The FTIR spectra of $BiFeO_3$, ZnS and different molar ratios of $BiFeO_3$/ZnS.

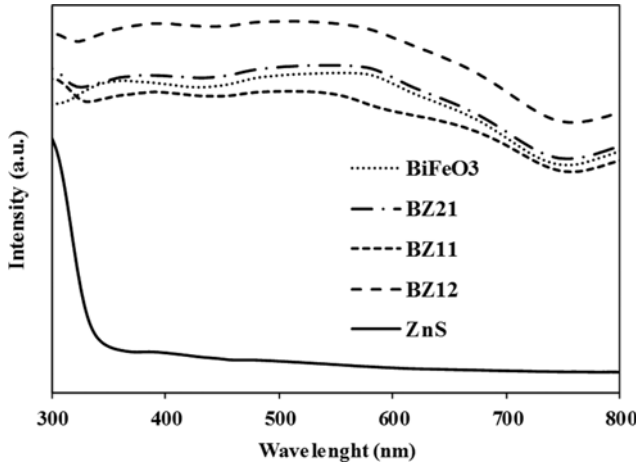

Fig. 4. The UV-vis spectra of $BiFeO_3$, ZnS and different molar ratios of $BiFeO_3$/ZnS.

reported results [18-20]. The peaks observed at a range of 1,488-1,640 cm^{-1} indicate the stretching models of C=O, and the absorption peaks observed at a range of 3,100-3,600 cm^{-1} indicate the stretching models of O-H which are involved in increasing water adsorption for -COOH nanocomposite group [16].

UV-vis analysis is used to find the wavelength range that a photocatalytic response is received. Fig. 4 shows the UV-Vis spectra of $BiFeO_3$, ZnS, BZ21, BZ11, and BZ12 samples in the range of 300-800 nm. As shown, pure ZnS is excited at 354 nm. This wavelength is fully in the ultraviolet A (UVA) region. Also, the $BiFeO_3$ wavelength was excited at about 548 nm, which is fully located in the visible region [21]. The spectra of the photocatalytic compounds clearly show that with increasing the $BiFeO_3$ content of photocatalyst, the light absorption spectrum extends to visible light. The excitation wavelengths of 427, 455, and 467 nm correspond to BZ12, BZ21, and BZ11 photocatalysts, respectively. The UV-vis spectrum also is used to extract other information such as the photocatalyst

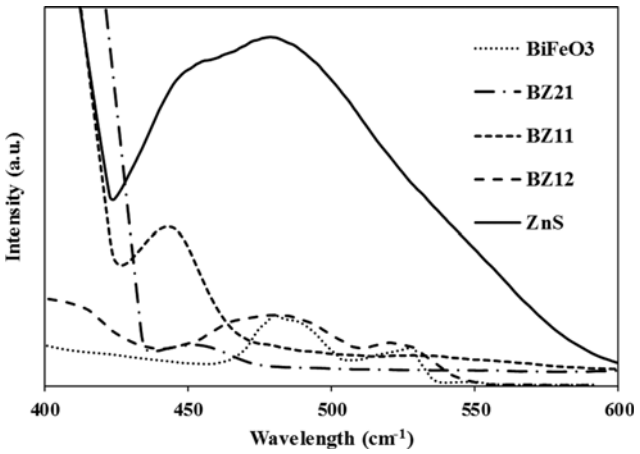

Fig. 5. The PL spectra of $BiFeO_3$, ZnS and different molar ratios of $BiFeO_3$/ZnS.

band gap energy. The experimental Eq. (2) was used to calculate the photocatalyst band gap energy with a good approximation [11].

$$E_g = 1240/\lambda \quad (2)$$

where E_g is the photocatalyst band gap, and λ is the photocatalyst wavelength of excitation. According to Eq. (2), the band gap energies of $BiFeO_3$, ZnS, BZ12, BZ21, and BZ11 photocatalysts were estimated to be 2.26, 3.5, 2.9, 2.72, and 2.65 eV, respectively. Thus, among the coupled photocatalysts, BZ11 had the best performance in absorption of visible-light photons.

The PL spectrum shown in Fig. 5 presents some information on the rate of charge separation efficiency in the semiconductors. It is believed that the surface area under the curve of PL analysis indicates the released energy caused by recombination of charge carriers so that the higher recombination rate, the larger surface area. Accordingly, the highest and lowest charge separation efficiencies belong to the pure $BiFeO_3$ and ZnS, respectively. Generally, being narrow the band gap of photocatalyst resulted in high rate recombination of charge carries because the attraction forces made in the activated narrow band gap photocatalyst is greater than a wide band gap photocatalyst. But, In spite of this fact, $BiFeO_3$ which had the limited band gap of 2.26 eV showed the highest efficiency of charge separation. It follows from this finding that $BiFeO_3$ well supplied electrons but they do not have enough energy to initiate CO_2 conversion reactions. Coupling ZnS with $BiFeO_3$ is a proper strategy to overcome this issue by upgrading the potential level of these low-energy electrons. In the coupled samples, it can be seen that with increasing $BiFeO_3$ content, the life time of charge carriers increased. Thus, the best coupled sample is BZ21.

2. Photocatalytic Reduction of CO_2

Fig. 6 shows the schematic energy levels of $BiFeO_3$ and ZnS photocatalysts. When $BiFeO_3$ and ZnS photocatalysts are in contact with each other, because of electrostatic forces between opposite loads charges, a load a charge density slope gradient is created at the borderline of the semiconductors and a Fermi level balance occurs. This Fermi level balance leads to promoting potential level of conduction band of $BiFeO_3$. Thus, the excited electrons of $BiFeO_3$ which is coupled with ZnS are more energetic than those of pure

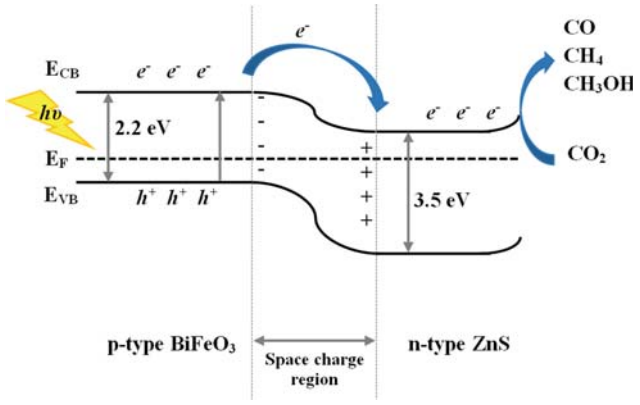

Fig. 6. Schematic energy levels of $BiFeO_3$ and ZnS after connection and load transfer process.

$BiFeO_3$. In addition, the p-n junction make an internal electric field in the interface of two photocatalysts. This electric field is oriented from n-type photocatalyst to the p-type one forces the excited electrons of $BiFeO_3$ in the opposite direction of the internal electric field, from conduction band of $BiFeO_3$ to conduction band of ZnS. This means that the life time of electron-holes is increased significantly. In general, the p-n junction of $BiFeO_3$/ZnS resulted in two positive effects. First, upgrading potential level of excited electrons of $BiFeO_3$ which is needed for appropriate reduction of CO_2; second, increasing life time of charge carriers by transfer of electrons from conduction band of $BiFeO_3$ to the conduction band of ZnS due to inner electric field made in p-n interface which forces electrons to be moved in opposite direction of electric field.

Fig. 7 presents the results of photocatalytic conversion of CO_2 by $BiFeO_3$, ZnS, and the coupled samples after 270 min experiment under visible light irradiation. The lowest visible light photocatalytic conversion of CO_2 belongs to ZnS by 3.2%. This behavior may be due to high electron mobility of ZnS. $BiFeO_3$ showed photocatalytic conversion of 7.36% under visible light. Despite being visible-light active photocatalyst, $BiFeO_3$ is not able to reduce CO_2 significantly because its generated electrons do not have enough energy as discussed earlier. At the same time with the reduction

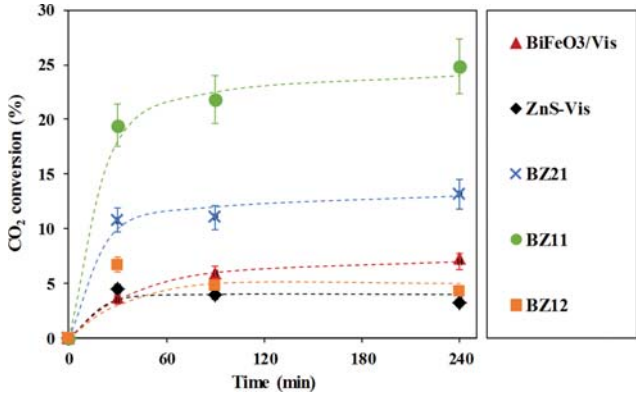

Fig. 7. The photodegradation percentage of CO_2 in the presence of pure $BiFeO_3$, ZnS and different molar ratios of $BiFeO_3$: ZnS, after 4 h of experimentation.

process, the holes generated in the valence band of $BiFeO_3$, which have enough potential for oxidation process, initiate the oxidizing reactions of CH_4. The oxidation reactions lead to consumption of holes and thus the density of electrons in the conduction band of pure $BiFeO_3$ will increase. These dense electrons could give their energy to each other, and thus some electrons with enough energy are generated to reduce the target CO_2 [22,23]. By coupling $BiFeO_3$ with ZnS, the photocatalytic efficiency of CO_2 conversion was increased significantly. One can see that BZ11 as the efficient sample showed the best photocatalytic conversion of CO_2, 24.8%, under visible light. This result is in agreement with the interpretation of Fig. 6. Considering the PL and UV-vis analyses, the best coupled sample for absorption of visible light photons and for separation of charge carriers is BZ21. But the results of photoreactor experiments indicated only 16.13% CO_2 conversion by BZ21 sample, which is lower than that of BZ11. This behavior can be attributed to the effect of p-n structure. When coupled photocatalyst includes an equimolar ratio of two photocatalysts, the p-n structure is promoted and its positive effects resulted in effective conversion of CO_2. But the p-n structure vanished gradually in the coupled samples with non-equimolar ratio of photocatalysts [24].

One can see from Fig. 7 that the photocatalytic reactions were saturated with passing time. The saturation in the conversion of CO_2 may be due to two reasons. (1) The product accumulation on catalysts surface caused by not being desorption of surface products. (2) The backward reactions leading to reoxidizing photocatalytic products back into CO_2. This phenomenon happens in the presence of O_2 and O_2 is an inevitable product of CO_2 conversion. Thus, it is reasonable that the photocatalytic conversion of CO_2 is saturated after a while. By literature review and our previous experimental researches [25-27], the decreasing concentration of CO_2 could be attributed to formation of C_1-based products like CO, CH_4, CH_3OH. Although, the published researches and the proposed mechanisms in reference [28] showed that the formation of methane in gaseous media is more probable than the formation of methanol and methanol seems to be the dominant product of aqueous media. Eqs. (3) to (11) propose a reaction route for production of the main C_1-based products by simultaneous oxidation of CH_4 as reductant agent and reduction of CO_2.

$$CO_2+e^- \rightarrow {}^{\bullet}CO_2^- \quad (3)$$

$$CH_4+h^+ \rightarrow {}^{\bullet}CH_3+H^+ \quad (4)$$

$$H^++e^- \rightarrow {}^{\bullet}H \quad (5)$$

$${}^{\bullet}H+{}^{\bullet}CO_2^- \rightarrow CO+{}^{\bullet}OH \quad (6)$$

$$CO+e^- \rightarrow {}^{\bullet}CO^- \quad (7)$$

$${}^{\bullet}CO^-+{}^{\bullet}H \rightarrow {}^{\bullet}C+OH^- \quad (8)$$

$${}^{\bullet}C+3{}^{\bullet}H \rightarrow {}^{\bullet}CH_3 \quad (9)$$

$${}^{\bullet}CH_3+{}^{\bullet}H \rightarrow CH_4 \quad (10)$$

$${}^{\bullet}CH_3+{}^{\bullet}OH \rightarrow CH_3OH \quad (11)$$

CONCLUSION

Different molar ratios of $BiFeO_3$/ZnS composite were synthe-

sized by hydrothermal and precipitation methods and used for direct photocatalytic conversion of CO_2 under visible light. The results of characterization analyses showed the good synthesis of the photocatalysts and desirable optical features in the absorption of UV light irradiation. The highest visible-light photocatalytic conversion of CO_2 was 24.8% by BZ11 sample. This behavior is attributed to the effect of p-n junction in promoting charge separation efficiency caused by internal electric field made in interface of two photocatalysts.

REFERENCES

1. X. Chang, J. Zheng, M. A. Gondal and G. Ji, *Res. Chem. Intermed.*, **41**(2), 739 (2015).
2. H. Rodhe, *Science*, **248**, 1217 (1990).
3. Y. Im, J. H. Lee and M. Kang, *Korean J. Chem. Eng.*, **34**(6), 1669 (2017).
4. W. Subramonian, T. Y. Wu and S.-P. Chai, *J. Environ. Manage.*, **187**, 298 (2017).
5. C. Y. Teh, T. Y. Wu and J. C. Juan, *Chem. Eng. J.*, **317**, 586 (2017).
6. Z. Qin, H. Tian, T. Su, H. Ji and Z. Guo, *RSC Adv.*, **6**, 52665 (2016).
7. N. Nuraje and K. Su, *Nanoscale*, **5**, 8752 (2013).
8. J. K. Kim, S. S. Kim and W. J. Kim, *Mater. Lett.*, **59**, 4006 (2005).
9. T. Gao, Z. Chen, Y. Zhu, F. Niu, Q. Huang, L. Qin, X. Sun and Y. Huang, *Mater. Res. Bull.*, **59**, 6 (2014).
10. T. Baran, S. Wojtyla, A. Dibebedetto, M. Aresta and W. Macyk, *Appl. Catal. B*, **178**, 170 (2015).
11. Y. Zhang, A. M. Schultz, P. A. Salvador and G. S. Rohrer, *J. Mater. Chem.*, **21**, 4168 (2011).
12. W. Ramadan, P. A. Shaikh, S. Ebrahim, A. Ramadan, B. Hannoyer, S. Jouen, X. Sauvage and S. Ogale, *J. Nanopart. Res.*, **15**, 1848 (2013).
13. S. Kaur, S. Sharma and S. K. Kansal, *Superlat. Microstruct.*, **98**, 86 (2016).
14. L. Kashinath, K. Namratha and K. Byrappa, *J. Alloy. Compoun.*, **695**, 799 (2017).
15. W. Ramadan, P. A. Shaikh, S. Ebrahim, A. Ramadan, B. Hannoyer, S. Jouen, X. Sauvage and S. Ogale, *J. Nanopartic. Res.*, **15**, 1848 (2013).
16. P. Iranmanesh, S. Saeednia and M. Nourzpoor, *Chin. Phys. B*, **24**(4), 046104 (2015).
17. B. Matovic, J. Pantic, J. Lukovic, M. Cebela, S. Dmitrovic, M. Mirkovic and M. Prekajski, *Ceram. Int.*, **42**, 615 (2016).
18. Y. Zhang, A. Zheng, X. Yang, H. He, Y. Fan and C. Yao, *Cryst. Eng. Comm.*, **14**, 8432 (2012).
19. K. K. Som, S. Molla, K. Bose and B. K. Chaudhuri, *Phys. Rev. B*, **45**, 4 (1992).
20. G. S. Lotey and N. K. Verma, *Mater. Sci. Semiconduc. Proces.*, **21**, 206 (2014).
21. M. Čebela, D. Zagorac, K. Batalović, J. Radaković, B. Stojadinović, V. Spasojević and R. Hercigonja, *Ceram. Int.*, **43**, 1256 (2017).
22. R. Yousefi, B. Kamaluddin, M. Ghoranneviss and F. Hajakbari, *Appl. Surf. Sci.*, **255**, 6985 (2009).
23. T. Soga, *Nanostructured materials for solar energy conversion*, Elsevier. 1st Ed. (2006).
24. L. Li, P. A. Salvador and G. S. Rohre, *Nanoscale*, **6**, 24 (2014).
25. N. Yazdanpour and S. Sharifnia, *Sol. Energy Mater. Sol. Cells*, **118**, 1 (2013).
26. G. Mahmodi, S. Sharifnia, M. Madani and V. Vatanpour, *Solar Energy*, **97**, 186 (2013).
27. M. Torabi Merajin, S. Sharifnia, S. N. Hosseini and N. Yazdanpour, *J. Taiwan Inst. Chem. Eng.*, **44**, 239 (2013).
28. E. Karamian and S. Sharifnia, *J. CO_2 Util.*, **16**, 194 (2016).